Electronic Supplementary Material

Hollow Manganese Phosphate Nanoparticles as Smart Multifunctional Probes for Cancer Cell Targeted Magnetic Resonance Imaging and Drug Delivery

Jing Yu[1], Rui Hao[1], Fugeng Sheng[2] (✉), Lili Xu[2], Gongjie Li[2], and Yanglong Hou[1] (✉)

[1] Department of Materials Science and Engineering, College of Engineering, Peking University, Beijing 100871, China
[2] Department of Radiology, Affiliated Hospital of the Academy of Military Medical Sciences, Beijing 100071, China

Supporting information to DOI 10.1007/s12274-012-0252-z

Figure S-2 shows the FTIR spectra of APS–PEG–COOH and APS–PEG–FA. As shown in Fig. S-2(a), the emergence of peaks at 1026 cm^{-1} and 879 cm^{-1} corresponding to Si–O–C stretching bands confirms the presence of APS in APS–PEG–COOH. The peaks at 1105 cm^{-1} and 1341 cm^{-1} most probably arise from C–O–C stretching and anti-symmetric stretching vibrations from the PEG [1]. Bands at 2930 cm^{-1}, 2881 cm^{-1}, and 1460 cm^{-1} arise from the anti-symmetric, symmetric stretching, and bending bands of $–CH_2–$. A broad –OH stretching band centered at 3367 cm^{-1} arising from the PEG diacid is also present. The peak at 1778 cm^{-1} is characteristic of the carbonyl stretching band of PEG diacid. These peaks show the successful chemical bonding of PEG diacid to APS. After binding FA with APS–PEG–COOH (Fig. S-2(b)) a peak at 789 cm^{-1}, which can be attributed to N–H out of plane wagging of FA, was observed. Meanwhile, the N–H bending band from –CONH– at 1608 cm^{-1} and the C–H aromatic stretching band at 3050 cm^{-1} increased in absorbance, further confirming the formation of APS–PEG–FA [2].

TG/DTG plots of APS–PEG–COOH and APS–PEG–FA were obtained when using the optimum conditions, with a heating rate of 10 ℃·min^{-1} at a flow rate of 60 mL·min^{-1} of dry nitrogen gas. Figure S-3(a) shows the TG/DTG trace for APS–PEG–COOH. A mass loss occurred around 100 ℃ due to the loss of adsorbed water [3]. The peaks at 420 ℃ can be attributed to the decomposition of the intercalated APS while the peak at 533 ℃ corresponds to the decomposition of the grafted APS [4, 5]. The peak at 389 ℃ can be attributed to the decomposition of PEG diacid. These data confirm the linkage between APS and PEG diacid. Figure S-3(b) shows the TG/DTG image of APS–PEG–FA. Comparison with Fig. S-3(a) shows there are additional peaks at 351 ℃, 465 ℃, and 571 ℃, which can be attributed to the decomposition of FA [6], confirming the successful synthesis of APS–PEG–FA.

Address correspondence to Yanglong Hou, hou@pku.edu.cn; Fugeng Sheng, shengfugeng@gmail.com

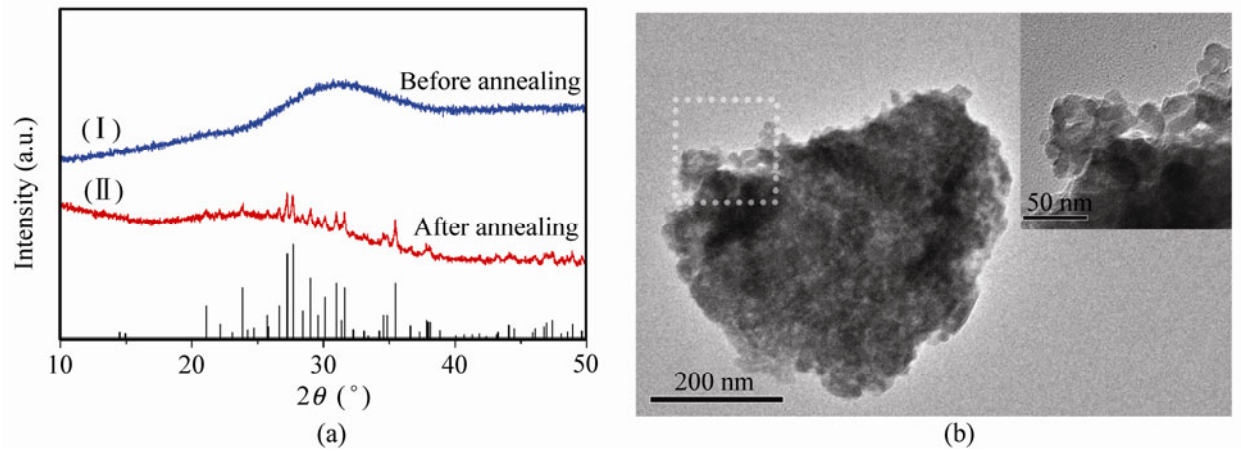

Figure S-1 (a) XRD patterns of HMP NPs (Ⅰ) before and (Ⅱ) after annealing at 500 ℃ for 2 h. (b) TEM image of HMP NPs after annealing at 500 ℃ for 2 h

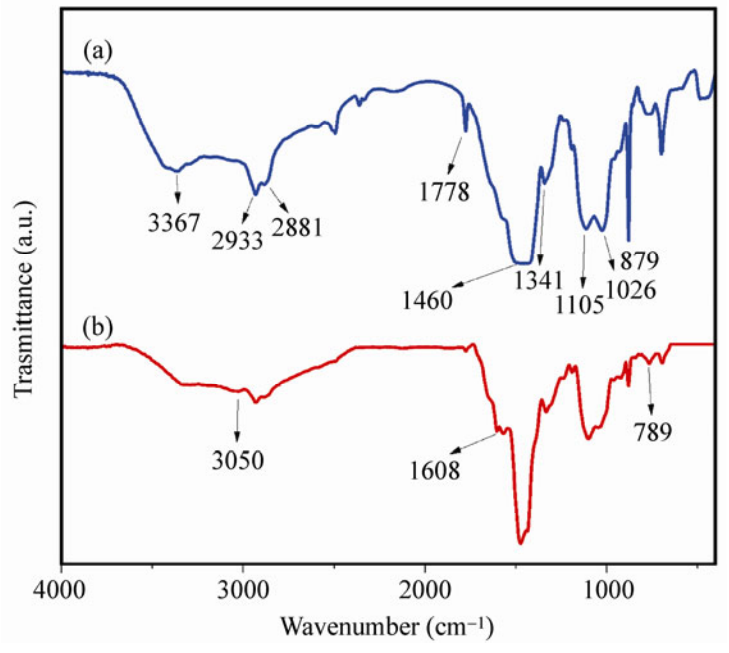

Figure S-2 FTIR spectra of (a) APS–PEG–COOH and (b) APS–PEG–FA

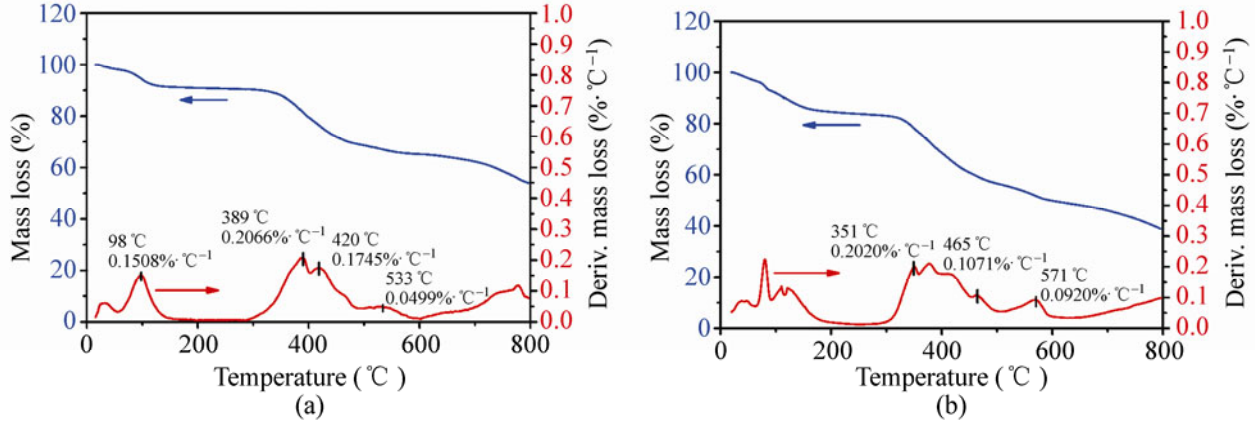

Figure S-3 TG/DTG traces of (a) APS–PEG–COOH and (b) APS–PEG–FA

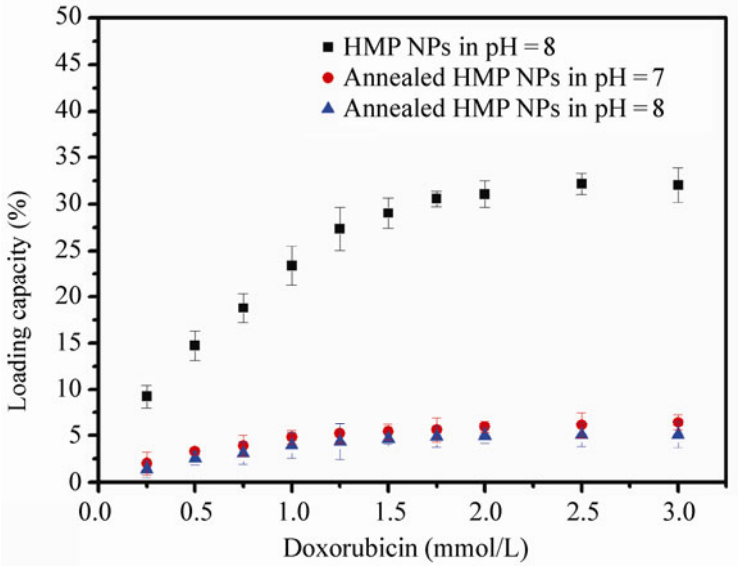

Figure S-4 Quantification of DOX loading capacity of HMP NPs before annealing at different DOX concentrations at pH 7 and HMP NPs before annealing at different DOX concentrations at pH 8. Error bars are based on standard deviations of triplicated samples

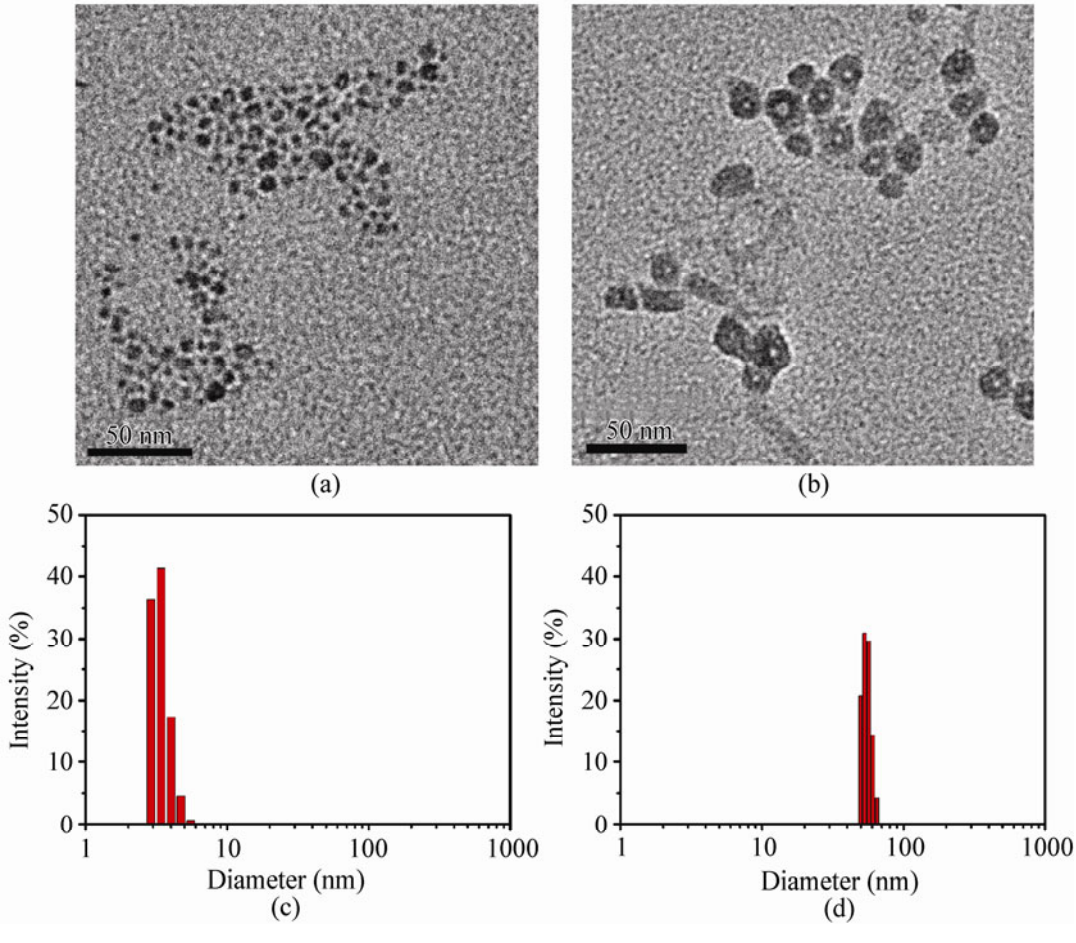

Figure S-5 TEM images of HMP NPs dispersed in (a) pH 5.4 and (b) pH 7.4 buffer solutions. Hydrodynamic size distribution of HMP NPs dispersed in (c) pH 5.4 and (d) pH 7.4 buffer solutions monitored by DLS

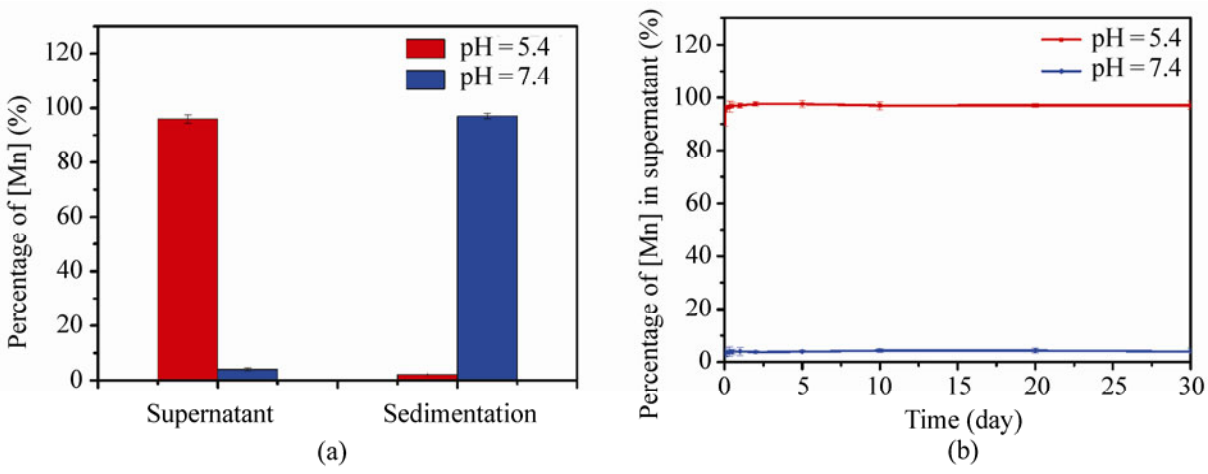

Figure S-6 (a) Manganese content in supernatant and sedimentation of HMP after centrifugation with 15 000 r/min at pH 5.4 and pH 7.4. (b) Manganese concentration in the supernatant at pH 5.4 and 7.4 at 30 days after centrifugation

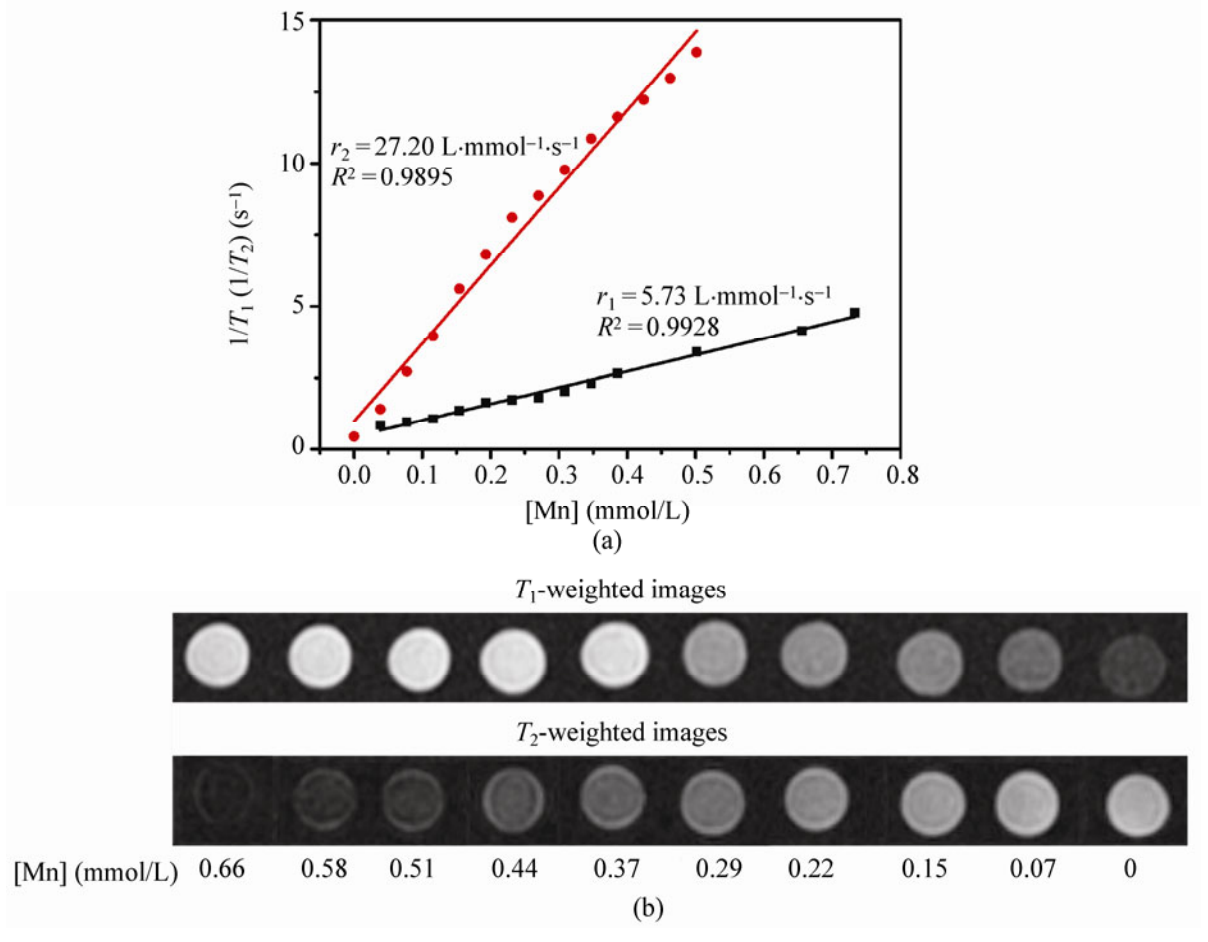

Figure S-7 (a) Plots of T_1^{-1} and T_2^{-1} versus manganese concentration for $MnCl_2$. (b) T_1- and T_2-weighted images for $MnCl_2$ in a 1.5 T MRI system

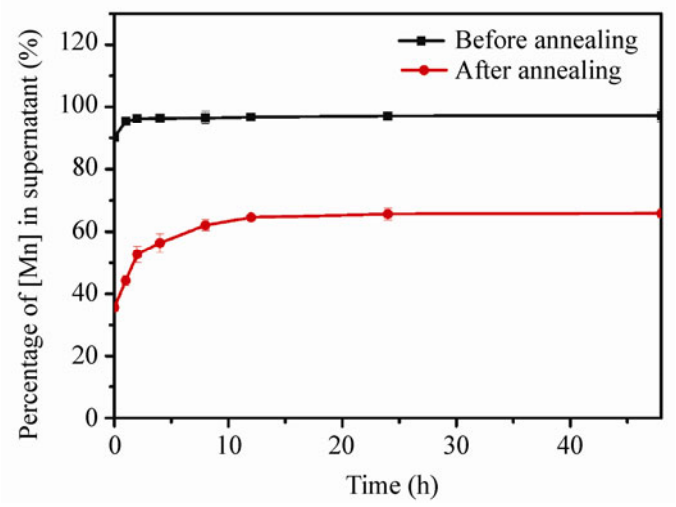

Figure S-8 Manganese concentration in supernatant of HMP at pH 5.4 before and after annealing at 500 ˚C. The supernatant was obtained after centrifugation at 15 000 r/min for 30 min

References

[S-1] Larsen, E. K. U.; Nielsen, T.; Wittenborn, T.; Birkedal, H.; Vorup-Jensen, T.; Jakobsen, M. H.; Ostergaard, L.; Horsman, M. R.; Besenbacher, F.; Howard, K. A. et al. Size-dependent accumulation of PEGylated silane-coated magnetic iron oxide nanoparticles in murine tumors. *ACS Nano* **2009**, *3*, 1947–1951.

[S-2] Morelli, C.; Maris, P.; Sisci, D.; Perrotta, E.; Brunelli, E.; Perrotta, I.; Panno, M. L.; Tagarelli, A.; Versace, C.; Casula, M. F. et al. PEG-templated mesoporous silica nanoparticles exclusively target cancer cells. *Nanoscale* **2011**, *3*, 3198–3207.

[S-3] Vora, A.; Riga, A.; Dollimore, D.; Alexander, K. Thermal stability of folic acid in the solid-state. *J. Therm. Anal. Calorim.* **2004**, *75*, 709–717.

[S-4] Shen, W.; He, H.; Zhu, J.; Yuan, P.; Frost, R. L. Grafting of montmorillonite with different functional silanes via two different reaction systems. *J. Colloid Interface Sci.* **2007**, *313*, 268–273.

[S-5] He, H.; Duchet, J.; Galy, J.; Gerard, J. F. Grafting of swelling clay materials with 3-aminopropyltriethoxysilane. *J. Colloid Interface Sci.* **2005**, *288*, 171–176.

[S-6] Abd El-Wahed, M. G.; Refat, M. S.; El-Megharbel, S. M. Synthesis, spectroscopic and thermal characterization of some transition metal complexes of folic acid. *Spectrochim. Acta, Part A* **2008**, *70*, 916–922.